PAPER

Percentile-specific computational phantoms constructed from ICRP mesh-type reference computational phantoms (MRCPs)

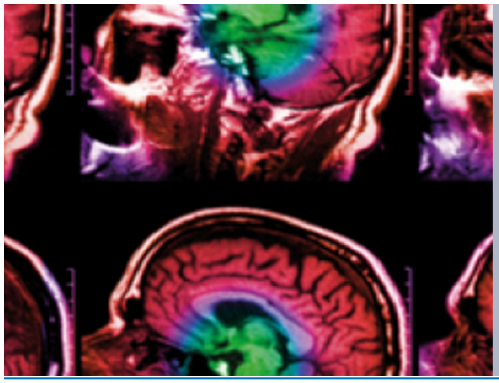

IOP Publishing Phys. Med. Biol. 64 (2019) 045005 (20pp) https://doi.org/10.1088/1361-6560/aafcdb

Physics in Medicine & Biology

IPEM Institute of Physics and Engineering in Medicine

PAPER

Percentile-specific computational phantoms constructed from ICRP mesh-type reference computational phantoms (MRCPs)

Hanjin Lee[1], Yeon Soo Yeom[2], Thang Tat Nguyen[3], Chansoo Choi[1], Haegin Han[1], Bangho Shin[1], Xujia Zhang[1], Chan Hyeong Kim[1,6], Beom Sun Chung[4] and Maria Zankl[5]

[1] Department of Nuclear Engineering, Hanyang University, 222 Wangsimni-ro, Seongdong-gu, Seoul 04763, Republic of Korea
[2] Division of Cancer Epidemiology & Genetics, National Cancer Institute, 9609 Medical Center Drive, Bethesda, MD 20892-9760, United States of America
[3] School of Nuclear Engineering and Environmental Physics, Hanoi University of Science and Technology, 1 Dai Co Viet road, Hai Ba Trung District, Hanoi, Vietnam
[4] Department of Anatomy, Ajou University School of Medicine, 164 Worldcup-ro, Suwon, Gyeonggi-do 16499, Republic of Korea
[5] Helmholtz Zentrum München German Research Center for Environmental Health, Institute of Radiation Protection, Ingolstädter Landstraße 1, 85764 Neuherberg, Germany
[6] Author to whom any correspondence should be addressed.

E-mail: chkim@hanyang.ac.kr

RECEIVED
26 September 2018

REVISED
21 December 2018

ACCEPTED FOR PUBLICATION
7 January 2019

PUBLISHED
5 February 2019

Keywords: mesh-type reference computational phantom, non-reference phantom, percentile-specific phantom, body size, Monte Carlo

Abstract

Recently, the Task Group 103 of the International Commission on Radiological Protection (ICRP) has developed new mesh-type reference computational phantoms (MRCPs) for adult male and female. When compared to the current voxel-type reference computational phantoms in ICRP Publication 110, the MRCPs have several advantages, including deformability which makes it possible to create phantoms in different body sizes or postures. In the present study, the MRCPs were deformed to produce a set of percentile-specific phantoms representing the 10th, 50th and 90th percentiles of standing height and body weight in Caucasian population. For this, anthropometric parameters for the percentile-specific phantoms were first derived from the anthropometric software and survey data. Then, the MRCPs were modified to match the derived anthropometric parameters. For this, first, the MRCPs were scaled in the axial direction to match the head height, torso length, and leg length. Then, the head, torso, and legs were scaled in the transversal directions to match the lean body mass for the percentile-specific phantoms. Finally, the scaled phantoms were manually adjusted to match the body weight and the remaining anthropometric parameters (upper arm, waist, buttock, thigh, and calf circumferences and sagittal abdominal diameter). The constructed percentile-specific phantoms and the MRCPs were implemented into the Geant4 Monte Carlo code to calculate organ doses for a cesium-137 contaminated floor. The results showed that organ doses of the 50th percentile (both standing height and body weight) phantoms are very close to those of the MRCPs. There were noticeable differences in organ doses, however, for the 10th and 90th percentile phantoms when compared with those of the MRCPs. The results of the present study confirm the general intuition that a small person receives higher doses than a large person when exposed to a static radiation field, and organs closer to the source receive higher doses.

1. Introduction

To perform an individualized dosimetry for retrospective dose reconstruction (Clairand *et al* 2008, Courageot *et al* 2010, Lu *et al* 2017) or virtual calibration of counters (Pierrat *et al* 2005, Bochud *et al* 2014, Chen *et al* 2016) based on Monte Carlo modeling, it would be ideal to use a computational human phantom which is directly produced using a tomographic image (i.e. from computed tomography (CT) or magnetic resonance imaging (MRI)) of the individual of interest. For most cases, however, it is neither practical nor necessary to directly produce a computational phantom for the individual considering that it will require not only a CT or MRI imaging for the individual, but also time-consuming phantom construction. Therefore, it is considered as a

practical solution to modify existing computational phantoms to create phantoms with various body sizes in advance and to use one of the phantoms which best fits the individual (Geyer *et al* 2014, Akhavanallaf *et al* 2018).

Several research groups (Johnson *et al* 2009, Na *et al* 2010, Cassola *et al* 2011, Ding *et al* 2012, Geyer *et al* 2014) have modified their own existing phantoms to construct different-size or percentile-specific phantoms. For example, Cassola *et al* (2011) modified the MASH3 and FASH3 phantoms to construct 18 phantoms which represent 10th, 50th, and 90th percentile standing height and body weight in male and female Caucasian populations. Na *et al* (2010) modified the RPI-AM and RPI-AF phantoms to construct percentile-specific phantoms. The RPI-AM and RPI-AF phantoms were also modified to construct a set of obese phantoms with 5 different body weights with the same standing height for each gender considering both subcutaneous and visceral adipose tissue growth (Ding *et al* 2012). Johnson *et al* (2009) developed a methodology to construct percentile-specific phantoms for the UF/NCI family of hybrid phantoms and constructed 25 different adult male and 15 pediatric female phantoms for US population for the purpose of demonstrating the methodology. Extending the work of Johnson *et al* (2009) and Geyer *et al* (2014) established a phantom library, containing 193 adult and 158 pediatric phantoms, to cover the body sizes of the entire US population.

Recently, the International Commission on Radiological Protection (ICRP) Task Group 103 developed new adult male and female mesh-type reference computational phantoms (MRCPs) (Kim *et al* 2018). The MRCPs were constructed by converting the current voxel-type reference computational phantoms (VRCPs) of ICRP Publication 110 (ICRP 2009) into a high-quality/fidelity mesh format, addressing the limitations of the VRCPs due to their limited voxel resolutions and the nature of voxel geometry. The MRCPs include all the source and target organs/tissues required for effective dose calculation, including the micron-scale regions such as the stem cell layers in the alimentary and respiratory tract organs which were not modelled in the VRCPs. Note that the MRCPs can be directly used in Monte Carlo codes for dose calculation where the advantages of mesh geometry are fully maintained, while a so-called 'voxelization' process is required for most existing mesh phantoms (Kim *et al* 2018, Yeom *et al* 2014). In addition, the mesh geometry of the MRCPs provides deformability, which encouraged us to deform the phantoms to non-reference-size phantoms with different body sizes to be used for individualized dosimetry.

In the presented study, we modified the MRCPs to develop a total of 18 percentile-specific adult male and female phantoms that represent 10th, 50th and 90th percentile standing heights and body weights in male and female Caucasian populations. Prior to the modification, the standing height, body weight, and additional 10 anthropometric parameters were derived from the data extracted from the *PeopleSize 2008 Professional* software, the National Health and Nutrition Examination Survey (NHANES) database, and the US Army Anthropometric Survey (ANSUR II) database. The MRCPs were then scaled in the axial direction (i.e. z direction) of the body to match the derived values of head height, torso length, and leg length and in the transverse directions (i.e. x and y directions) to match the lean body mass (LBM) for the given standing height and body weight of the percentile-specific phantoms. The scaled phantoms were finally adjusted to match the body weight and the remaining anthropometric parameters (upper arm, waist, buttock, thigh, and calf circumferences and sagittal abdominal diameter). After the construction of the phantoms, the effect and validity of scaling and adjustments were investigated by calculating organ depth and cord length distributions and by comparing the organ masses with some available autopsy data. The constructed phantoms and the MRCPs were then implemented into the Geant4 Monte Carlo code to calculate organ doses for a cesium-137 contaminated floor, and the calculated values were compared to see the dosimetric influence of the differences in body sizes.

2. Materials and method

2.1. The mesh-type reference computational phantoms (MRCPs)

Figure 1 shows the adult male and female mesh-type reference computational phantoms (MRCPs) developed by the ICRP Task Group 103 (Kim *et al* 2018). The standing height and body weight of the MRCPs are consistent with the reference values of ICRP Publication 89 (2002) (i.e. male: 176 cm and 73 kg; female: 163 cm and 60 kg). The MRCPs contain 48 organs/tissues with 170 regions including those needed to calculate effective dose. The phantoms also include tens-of-micron-thick source and target regions in the eye lens, skin, urinary bladder, alimentary tract organs, and respiratory tract organs. The organ/tissue masses of the MRCPs are consistent with the reference values in ICRP Publications 89 (2002), inclusive of blood content, within 0.1% of deviation.

2.2. Derivation of anthropometric parameters

2.2.1. Standing height and body weight

In the present study, the adult MRCPs were modified to produce a set of percentile-specific phantoms which represent 10th, 50th and 90th percentile standing heights and body weights of adult male and female Caucasian populations. For this, first, the 10th, 50th and 90th percentile standing heights of male and female were extracted for each of the nine countries (i.e. Sweden, Netherlands, Germany, Belgium, Australia, USA, France, UK, and

Figure 1. MRCPs for adult male (left) and female (right).

Italy), following the approach used by Cassola *et al* (2011), from the *PeopleSize 2008 Professional* software (www.openerg.com), as shown in table 1. In the extracted data for each country, we selected the age group which is closest to the age range of adults (=20 to 50 years) considered in the ICRP Publication 89 (2002) (see table 1). Then, for each of the 10th, 50th and 90th percentile standing heights, the 10th, 50th and 90th percentile body weights were extracted, as shown in table 2. The extracted values of standing height and body weight were finally averaged for the nine countries, reflecting the population estimates of the 20–49 age group in 2015 provided in the UN World Population Prospects 2017 revision (UN-DESA 2017), to obtain the values of the 10th, 50th and 90th percentile standing heights and body weights for the entire Caucasian population.

2.2.2. Secondary anthropometric parameters

A total of ten additional anthropometric parameters (i.e. sitting height; head height, length, and breadth; sagittal abdominal diameter; and upper arm, waist, buttock, thigh, and calf circumferences) were derived to produce percentile-specific phantoms. Again, the *PeopleSize* software was used to derive the values of sitting height and head height for the percentile-specific phantoms assuming that these parameters depend only on standing height.

The value of sitting height, which is the 50th percentile value for the people with a given standing height percentile, was directly extracted from the *PeopleSize* software.

The head dimensions (i.e. height, length, and breadth) of the MRCPs were found to be significantly different from those derived from anthropometric data. For the head, therefore, we used a different approach. That is, in the present study, the head of the percentile-specific phantom was not directly matched to the head dimensions derived from anthropometric data, but adjusted for the same degree of change in head dimensions. For this adjustment, the head heights (i.e. from chin to top of head) were first determined for the standing heights of the percentile-specific phantom and the MRCP by linear regression of the head height data for the five countries (i.e. Germany, Belgium, Australia, USA, and UK) available in the *PeopleSize* software. Then, the head height for the percentile-specific phantom was calculated by multiplying the head height of the MRCP with the ratio of the head heights determined for the standing heights of the percentile-specific phantom and the MRCP. A similar approach was used to derive the values of head breadth and length for the percentile-specific phantom. The organs of the head were assumed to vary with the changes of the head dimensions. The main advantage of this ratio approach is that we can minimize the degree of scaling for the eyes, which are among the organs considered important in radiation protection; the change in the volume of the eye model was at most 11% and 13% for the male and female phantom, respectively.

Table 1. 10th, 50th, and 90th standing heights in male and female Caucasian populations. (Unit: centimeters.)

Country	Age group (years)	Standing height percentile					
		Male			Female		
		10th	50th	90th	10th	50th	90th
Sweden	18–65	169.5	178.6	187.6	158.7	167.6	176.4
Netherlands	18–64	169.9	179.2	188.6	158.2	166.1	173.9
Germany	20–50	168.7	177.8	186.8	157.7	166.2	174.7
Belgium	18–65	166.9	176.6	186.3	155.9	164.6	173.3
Australia	25–50	167.9	176.7	185.5	155.7	163.9	172.0
USA	25–50	167.3	177.0	186.6	154.6	163.1	171.6
France	18–70	166.7	175.6	184.5	154.2	162.5	170.8
UK	25–50	167.5	176.4	185.4	154.3	162.7	171.0
Italy	18–83	163.2	172.1	181.0	151.6	159.8	167.9

Table 2. 10th, 50th, and 90th body weights for people who have 10th, 50th, and 90th standing heights in Caucasian populations. (Unit: kilograms.)

Country	Standing height percentile	Body weight percentile					
		Male			Female		
		10th	50th	90th	10th	50th	90th
Sweden	10th	56	63	71	50	54	57
	50th	68	75	83	58	61	64
	90th	84	91	99	71	74	78
Netherlands	10th	60	67	73	52	56	59
	50th	71	77	84	61	65	69
	90th	85	91	98	77	81	85
Germany	10th	58	66	75	44	49	55
	50th	71	79	88	57	63	68
	90th	89	97	105	80	85	90
Belgium	10th	56	64	71	49	54	58
	50th	68	76	83	60	65	69
	90th	84	92	99	79	83	88
Australia	10th	62	70	78	46	51	57
	50th	75	83	91	59	65	70
	90th	92	100	108	82	88	93
USA	10th	55	65	76	43	50	57
	50th	72	82	93	60	67	74
	90th	95	105	116	90	97	104
France	10th	55	62	69	44	48	52
	50th	66	73	80	54	58	62
	90th	81	88	95	70	74	78
UK	10th	59	67	75	45	51	56
	50th	72	80	88	58	64	69
	90th	89	98	106	81	87	92
Italy	10th	52	59	67	45	48	51
	50th	64	71	78	53	56	59
	90th	79	87	94	65	68	71

The other anthropometric parameters depend not only on standing height but also on body weight, but the *PeopleSize* software does not provide anthropometric parameters as a function of multiple parameters; therefore, these anthropometric parameters were derived from other databases. The target values of upper arm, waist, buttock, thigh, and calf circumferences and sagittal abdominal diameter were derived from the data extracted from the National Health and Nutrition Examination Survey (NHANES) database which is a survey research program

conducted by the National Center for Health Statistics of the Centers for Diseases (www.cdc.gov/nchs/nhanes.html). Specifically, the data of the Continuous NHANES (1999–2014) database was used for sagittal abdominal diameter and upper arm, thigh, waist, and calf circumferences, and the data of the NHANES III (1988–1994) database was used for buttock circumference due to the absence of the data in the updated Continuous NHANES database. Head length and breadth, absent from the NHANES, were derived from the US Army Anthropometric Survey (ANSUR II) database which is the database of US Army subjects recently established by the Natick Soldier Research, Development and Engineering Center in 2012 (Gordon *et al* 2014). The values of these anthropometric parameters for the percentile-specific phantoms were derived from multiple linear regression of the data as a function of standing height and body weight.

2.3. Phantom construction

2.3.1. Scaling

In the present study, the values of the anthropometric parameters derived above serve as the target values to which the MRCPs are adjusted to produce percentile-specific phantoms. The percentile-specific phantoms were mainly constructed by scaling in the axial (i.e. z direction) and transversal directions (i.e. x and y directions), followed by manual adjustments for the skin (=exterior surface) and breasts to match the body weight and the remaining anthropometric parameters to the target values. For scaling, an MRCP was divided into three parts: head, torso (including arms), and legs. Then, each part was scaled separately. First, the head was scaled in the axial direction with the ratio method explained earlier. Then, the torso was scaled in the axial direction to match the sitting height (=torso length + head height) of the phantom to the target value of sitting height. Finally, the legs were scaled in the axial direction to match the target values of leg length.

After scaling in the axial direction, the MRCP was scaled in the transverse directions. In the present study, the torso and legs were scaled using different scaling factors derived to match the lean body mass (LBM). Note that the LBM is the body weight devoid of the body fat, which is strongly correlated not only to internal organ/tissue mass (Bosy-Westphal 2004), but also to standing height and body weight (Hume 1966, James and Waterlow 1976, Boer 1984, Deurenberg *et al* 1991, Pieterman *et al* 2002). In the present study, the following equation (Deurenberg *et al* 1991, Pieterman *et al* 2002) was used to calculate the LBM for a given standing height and body weight of a percentile-specific phantom:

$$\mathrm{LBM} = W - \left[W \times \frac{1.2 \times \left(\frac{W}{H^2}\right) + 0.23 \times A - G}{100} \right] \tag{1}$$

where LBM is the lean body mass (kg), W is the body weight (kg), H is the standing height (cm), A is the age (years), and G is a gender-dependent parameter of 16.2 for male and 5.4 for female. This equation was derived based on the body fat data measured for 1229 subjects (male: 521 and female: 708) with a wide range in the age (7–83 years) and the body mass index (BMI: 13.9–40.9 kg m^{-2}) (Deurenberg *et al* 1991). Note that the LBM estimated with the equation using the standing height and body weight of the MRCP shows a good agreement with the LBM of the MRCP, for both the male and female phantom, the difference being only 0.16% and 0.36% for the male and female phantom, respectively. For the estimation, in the present study, the age (A) was assumed to be 35 years, the average value of the age range of adults considered in the ICRP Publication 89 (2002). In order to match the LBM in consideration of the torso or leg length, scaling factors in the transverse directions were derived for each part, following the approach used by Qiu *et al* (2008). The torso including the arms was scaled in the transversal directions using a scaling factor calculated by the LBMs as follows:

$$\mathrm{SF}_{x,y}^{\mathrm{torso}} = \left(\frac{\mathrm{LBM}_{\mathrm{target}} \ / \ \mathrm{LBM}_{\mathrm{MRCP}}}{R_z^{\mathrm{torso}}} \right)^{0.5} \tag{2}$$

where $\mathrm{SF}_{x,y}^{\mathrm{torso}}$ is the scaling factor for the torso in the transversal directions, R_z^{torso} is the ratio of the target torso length and the MRCP torso length, $\mathrm{LBM}_{\mathrm{target}}$ is the LBM estimated for the target percentile-specific phantom, and $\mathrm{LBM}_{\mathrm{MRCP}}$ is the LBM of the MRCP.

Likewise, a scaling factor of the legs in the transversal directions was calculated by the following equation:

$$\mathrm{SF}_{x,y}^{\mathrm{legs}} = \left(\frac{\mathrm{LBM}_{\mathrm{target}} \ / \ \mathrm{LBM}_{\mathrm{MRCP}}}{R_z^{\mathrm{legs}}} \right)^{0.5} \tag{3}$$

where $\mathrm{SF}_{x,y}^{\mathrm{legs}}$ is the scaling factor for the legs in the transversal directions, R_z^{legs} is the ratio of the target leg length and the MRCP leg length.

For the scaling of the head in the transversal directions, the ratio approach was used which was previously used to scale the head in the axial direction. The head breadths (the maximum horizontal breadth of the head above the ears) were first determined for the target standing height and body weight and the MRCP standing height and body weight by multiple linear regression of the head height data as a function of standing height and

body weight. Then, the target head breadth was calculated by multiplying the MRCP head breadth by the ratio of the head breadths of the target standing height and body weight and the MRCP standing height and body weight. This approach was also used to derive the target value of head length (i.e. the distance from the glabella landmark between the brow ridges to opisthocranion).

The scaling approach using the scaling factors derived previously, however, resulted in slight dislocations at the boundaries of the body parts (head, torso, and legs) due to the differences in the transversal scaling factors for the head, torso, and legs. In the present study, therefore, the transversal scaling factors were modified to linearly change in the axial direction. That is, the scaling factor for the legs was modified to linearly change in the axial direction from the scaling factor of the torso (at the top of the legs) to the scaling factor of the legs (at the middle of the legs). For the head, the transversal scaling factor was modified to change linearly, from the scaling factor of the torso (at the bottom of the head) to the scaling factor of the head (at each measurement level of the head dimension), then from the scaling factor of the head (at each measurement level of the head dimension) to unity (at the top of the head).

2.3.2. *Adjustment for skin and breasts*

After the scaling of the phantom, the skin and breasts were adjusted manually as follows. For the skin, assuming that the skin mass is proportional to the body surface area, the target mass of the skin was determined using the following equation:

$$\mathrm{SM}_{\mathrm{target}}\,(\mathrm{kg}) = \mathrm{SM}_{\mathrm{MRCP}}\,(\mathrm{kg}) \times \mathrm{BSA}_{\mathrm{target}}\left(\mathrm{m}^2\right) / \mathrm{BSA}_{\mathrm{MRCP}}\left(\mathrm{m}^2\right) \tag{4}$$

where $\mathrm{SM}_{\mathrm{target}}$ and $\mathrm{BSA}_{\mathrm{target}}$ are the skin mass and body surface area of the target percentile-specific phantom, respectively, and $\mathrm{SM}_{\mathrm{MRCP}}$ and $\mathrm{BSA}_{\mathrm{MRCP}}$ are the skin mass and body surface area of the MRCP. The $\mathrm{BSA}_{\mathrm{target}}$ was calculated by using the following equation given in ICRP Publication 89 (2002):

$$\mathrm{BSA}\left(\mathrm{m}^2\right) = 0.0235 \times H^{0.42246} \times W^{0.51456} \tag{5}$$

where H is the standing height (cm) and W is the body weight (kg). Considering both the target skin mass and the target values of the remaining anthropometric parameters (i.e. upper arm, waist, buttock, thigh, and calf circumferences and sagittal abdominal diameter), the exterior skin surface was manually adjusted using the *Deform* function of the *Rapidform* software (INUS Technology Inc., Korea). Note that the deformed exterior skin surfaces of the phantoms were confirmed by a group of anatomists. Then, the deformed exterior skin surface was replicated to produce three additional surfaces. Then, one of the surfaces was reduced in size, by using the offset function of the software, to redefine the inner skin surface, exactly matching the target skin mass. The other two surfaces were also reduced to redefine the radiosensitive target layer in the skin at a depth of 50–100 μm from the exterior skin surface.

The breasts were finally adjusted assuming that the change in the mass of breast adipose tissue is directly proportional to that of the residual soft tissue (RST) which is mainly composed of adipose tissue. That is, the breasts of the scaled phantom were adjusted to preserve the ratio of the masses of the breast adipose tissue to RST of the MRCP. In addition, following a recommendation of the anatomists, the breasts were slightly repositioned to preserve the ratio of the breast-center-to-skin and breast-center-to-muscle distances (in the anteroposterior direction) of the MRCP.

2.4. Monte Carlo dose calculations

The 10th, 50th, and 90th percentile phantoms (i.e. M_H10W10, M_H50W50, M_H90W90, F_H10W10, F_H50W50, and F_H90W90) which represent small, average, and large people, respectively, and the MRCPs were implemented in the Geant4 Monte Carlo code (ver. 10.03) (Allison *et al* 2016) to calculate the organ doses (=organ/tissue averaged absorbed doses) for the radiation exposure scenario described in Eakins (2015), in which cesium-137 is uniformly distributed on the surface of the floor (see figure 2). In this simulation, cesium-137 gammas were isotropically emitted on a disk of radius 200 cm below the feet of the phantom, using the *G4GeneralParticleSource*, and the phantom was assumed to be in air.

For implementation, the constructed percentile-specific phantoms in the polygonal-mesh format were first converted into tetrahedral-mesh format using the TetGen code (Si 2015), and then these phantoms were implemented in the Geant4 code by using the *G4Tet* class, following the method used in Yeom *et al* (2014). To transport photons and electrons, the electromagnetic physics library of *G4EmLivermorePhysics* was used with the secondary production cut value of 1 mm. The organ doses were calculated to have a relative error of less than 1% by transporting sufficient number of particles ($=4.2 \times 10^9$ particles). Variation reduction techniques (VRTs) were not used. Most organ/tissue doses were directly calculated using the *G4PSEnergyDeposit* class, but absorbed doses to the skeletal tissues (i.e. red bone marrow (RBM) and bone surface) were estimated by using the fluence-to-absorbed dose response functions (DRFs) in ICRP Publication 116 (2010).

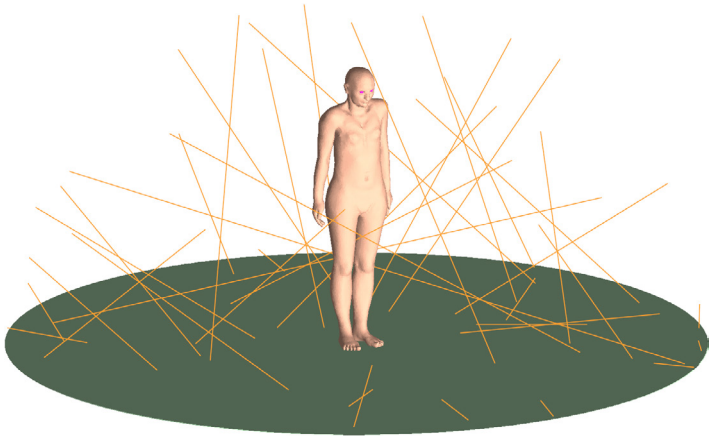

Figure 2. Monte Carlo simulation geometry for cesium-137 contamination on floor. Phantom is irradiated by photons isotropically emitted on disk of 200 cm radius below feet of phantom.

Table 3. 10th, 50th, and 90th percentile standing heights and body weights derived in present study for Caucasian adult population.

	Male			Female		
Percentile	Body weight 10th	Body weight 50th	Body weight 90th	Body weight 10th	Body weight 50th	Body weight 90th
Standing height 10th	167.2 cm 55.9 kg M_H10W10	167.2 cm 70.6 kg M_H10W50	167.2 cm 90.2 kg M_H10W90	154.9 cm 44.2 kg F_H10W10	154.9 cm 58.2 kg F_H10W50	154.9 cm 82.6 kg F_H10W90
Standing height 50th	176.5 cm 64.7 kg M_H50W10	176.5 cm 79.3 kg M_H50W50	176.5 cm 99.1 kg M_H50W90	163.3 cm 49.9 kg F_H50W10	163.3 cm 64.1 kg F_H50W50	163.3 cm 88.4 kg F_H50W90
Standing height 90th	185.8 cm 74.2 kg M_H90W10	185.8 cm 88.7 kg M_H90W50	185.8 cm 108.4 kg M_H90W90	171.7 cm 55.7 kg F_H90W10	171.7 cm 69.8 kg F_H90W50	171.7 cm 94.1 kg F_H90W90

3. Results and discussion

3.1. Percentile-specific anthropometric parameters

Table 3 shows the values of the 10th, 50th and 90th percentile standing heights and body weights derived in the present study for adult male and female to which the MRCPs were matched to produce percentile-specific phantoms. For standing height, it can be seen that the difference between 10th and 50th percentiles is close to the difference between 50th and 90th percentiles. For body weight, on the other hand, it can be seen that the difference between 10th and 50th percentiles is much smaller than the difference between 50th and 90th percentiles. This is mainly because the biologic lower limit of the body weight exists; that is, the body weight cannot be lower than the LBM which is a mass summation of internal organs/tissues excluding the adipose tissue (McArdle *et al* 2006). There is no biologic upper limit of the body weight. Comparing the MRCPs with the phantoms with the 50th percentile standing height and body weight, there is not much difference for standing height (male: 0.5 cm and female: 0.3 cm), while there is large difference in body weight; that is, the body weight of the MRCPs is less than those of the 50th percentile phantoms by 6.3 kg and 4.1 kg for the male and female phantom, respectively. Note that, according to the ICRP, the reference values do not represent mean or median values (ICRP 1975, 2002).

Table 4 shows the anthropometric parameters (i.e. sitting height; head height, length, and breadth; sagittal abdominal diameter; and upper arm, waist, buttock, thigh, and calf circumferences) derived in the present study by multiple linear regressions of the anthropometric parameters for percentile-specific phantoms. The adjusted coefficient of determination (R^2) of the regressions were high, i.e. greater than 0.77, for most parameters except for head length and breadth, for which the R^2 values were less than 0.19. Note that the size of the head does not significantly change with standing height or body weight, and individual variability is dominant. It was at least confirmed that the head length and breadth are correlated to standing height and body weight considering that the calculated p-value is smaller than 0.1.

Table 4. Anthropometric parameters derived in the present study.

	Standing height percentile	Body weight percentile	Sitting height (cm)	Head height (cm)	Head length (cm)	Head breadth (cm)	Sagittal abdominal diameter (cm)	Upper arm circumference (cm)	Waist circumference (cm)	Buttock circumference (cm)	Thigh circumference (cm)	Calf circumference (cm)
Male	10th	10th	88.5	22.8	19.3	15.0	17.3	28.7	77.2	85.9	46.2	33.9
		50th	88.5	22.8	19.5	15.3	20.3	31.8	88.7	94.0	50.7	36.7
		90th	88.5	22.8	19.8	15.6	24.2	35.9	104.0	104.8	56.9	40.4
	50th	10th	92.6	23.3	19.7	15.1	17.7	29.5	79.7	89.5	47.9	35.3
		50th	92.6	23.3	19.9	15.3	20.7	32.6	91.1	97.6	52.5	38.0
		90th	92.6	23.3	20.2	15.6	24.7	36.8	106.5	108.6	58.7	41.7
	90th	10th	96.6	23.8	20.0	15.2	18.3	30.5	82.7	93.6	49.9	36.7
		50th	96.6	23.8	20.2	15.4	21.2	33.6	94.0	101.6	54.5	39.5
		90th	96.6	23.8	20.5	15.7	25.2	37.7	109.4	112.5	60.6	43.2
Female	10th	10th	82.9	21.3	18.4	14.5	15.9	24.9	72.9	85.5	43.4	32.1
		50th	82.9	21.3	18.6	14.6	18.8	28.5	83.7	95.4	48.6	35.0
		90th	82.9	21.3	19.0	14.9	23.9	34.9	102.7	112.6	57.8	40.1
	50th	10th	86.6	21.7	18.7	14.6	15.7	25.1	73.9	87.8	44.6	33.2
		50th	86.6	21.7	18.9	14.7	18.7	28.8	84.9	97.8	49.9	36.1
		90th	86.6	21.7	19.3	15.0	23.8	35.1	103.7	114.9	59.1	41.2
	90th	10th	90.2	22.1	19.0	14.7	15.6	25.3	74.9	90.1	45.9	34.3
		50th	90.2	22.1	19.3	14.8	18.6	29.0	85.9	100.1	51.2	37.2
		90th	90.2	22.1	19.6	15.1	23.7	35.3	104.7	117.2	60.3	42.3

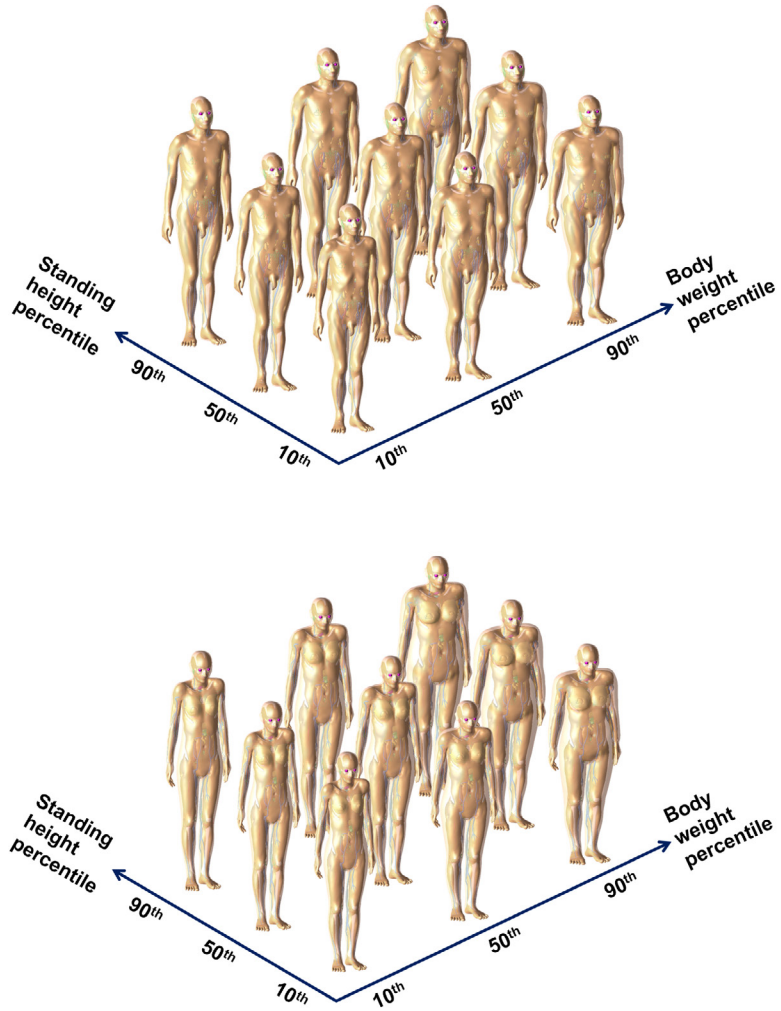

Figure 3. Constructed percentile-specific phantoms for male (upper) and female (lower).

3.2. Constructed percentile-specific computational phantoms

Figure 3 shows the percentile-specific phantoms which were constructed to represent the adult male and female of 10th, 50th and 90th percentiles in standing height and body weight. The constructed phantoms were exactly matched to the target values of standing height, body weight, head height and sitting height, i.e. <0.1% of difference. The phantoms also were matched to the target values of the other anthropometric parameters (i.e. upper arm, waist, buttock, thigh, and calf circumferences and sagittal abdominal diameter, listed in table 4) within 5% of difference. Tables 5 and 6 show the masses of the organs/tissues of the constructed phantoms for adult male and female, respectively, along with those of the MRCPs. Note that the masses of the most organs/tissues, except for the skin and breasts, were automatically determined during the scaling process. The masses of the skin and breasts were manually matched to the target values, the resulting differences being less than 0.1%.

3.3. Organ-depth and chord-length distributions

Figure 4 shows the organ-depth distributions (ODDs) of selected organs (spongiosa, colon wall, and brains) measured from the front, back, left, right, top, and bottom body surfaces for M_H10W10, M_H50W50, M_H90W90, F_H10W10, F_H50W50 and F_H90W90 percentile-specific phantoms. For the ODD calculation, 10^7 points were randomly sampled in the considered organ/tissue, and the distances from the sampled points to the outer surface (i.e. front, back, left, right, top, and bottom body surfaces) of the phantoms were calculated. The ODDs represent the depth of an organ/tissue below the outer surface of the phantoms, influencing dose calculation for external exposure. It can be seen that the ODDs for the spongiosa and colon wall show a similar trend; that is, for a given organ, a larger phantom shows a broader distribution, and the distributions are noticeably different for different percentile phantoms. Our analysis of the results indicates that the ODDs faithfully reflect the scaling of the phantoms in the axial and transversal directions. For the brain, except for the bottom direction, the differences in the ODDs were much smaller for different percentile phantoms, which reflects the fact that the head dimensions do not significantly change as a function of standing height and body weight. Note that, from the 10th percentile to the 90th percentile phantoms, considering both the male and female phantoms, the head

Table 5. Organ/tissue masses of constructed phantoms and the MRCP for adult male. Note that the organ/tissue masses are inclusive of blood content. (Unit: grams.)

Organ/tissue	M_H10W10	M_H10W50	M_H10W90	M_H50W10	M_H50W50	M_H50W90	M_H90W10	M_H90W50	M_H90W90	MRCP (male)
Adrenals	13.988	16.342	18.623	16.012	18.299	20.620	18.171	20.393	22.715	17.366
ET	35.914	39.178	42.487	38.744	41.864	45.181	41.723	44.717	47.995	40.874
Oral mucosa	0.114	0.127	0.140	0.123	0.136	0.148	0.134	0.145	0.158	0.132
Trachea	8.348	9.753	11.114	9.556	10.921	12.306	10.844	12.170	13.556	10.364
BB_1	2.557	2.987	3.403	2.926	3.344	3.769	3.321	3.727	4.151	3.173
Arteries	268.719	314.367	358.482	308.159	352.640	397.368	350.145	392.972	438.254	336.000
Veins	803.339	940.689	1076.133	259.292	1057.640	1192.713	1048.454	1177.205	1315.097	1008.000
Skeletal system	8135.244	9376.760	10585.302	9207.878	10412.774	11641.496	10349.606	11519.123	12746.623	9913.516
Brain	1431.537	1473.356	1523.986	1493.197	1534.699	1586.648	1557.758	1599.093	1651.645	1517.390
Breasts, glandular	8.345	9.750	11.110	9.553	10.917	12.302	10.841	12.166	13.552	10.360
Breasts, adipose	9.658	16.224	27.064	12.570	18.659	29.579	14.608	21.348	32.189	15.538
Eye	14.370	15.021	15.759	15.140	15.774	16.524	15.948	16.569	17.322	15.542
Gallbladder wall	8.348	9.753	11.114	9.556	10.921	12.306	10.844	12.170	13.556	10.364
Gallbladder contents	46.720	54.582	62.199	53.479	61.118	68.871	60.691	68.111	75.865	58.000
Stomach wall	156.490	182.823	208.334	179.128	204.714	230.684	203.283	228.136	254.111	194.271
Stomach contents	201.381	235.268	268.097	230.514	263.439	296.860	261.598	293.580	327.006	250.000
Small intestine wall	694.846	811.769	925.042	795.365	908.970	1024.285	902.617	1012.969	1128.303	862.599
Small intestine contents	281.934	329.375	375.336	322.719	368.815	415.603	366.237	411.012	457.809	350.000
Colon wall	397.157	463.968	528.731	454.611	519.544	585.456	515.854	578.988	644.748	493.040
Colon contents	241.657	282.322	321.716	276.617	316.127	356.232	313.917	352.296	392.408	300.000
Heart wall	310.803	363.102	413.769	355.765	406.580	458.160	403.738	453.098	504.687	385.839
Blood in heart	410.818	479.947	546.918	470.248	537.416	605.594	533.660	598.904	667.093	510.000
Kidneys	340.049	397.270	452.705	389.242	444.839	501.273	441.730	495.735	552.178	422.145
Liver	1901.039	2220.930	2530.836	2176.050	2486.865	2802.355	2469.483	2771.397	3086.941	2360.000
Lungs	965.614	1128.099	1285.513	1105.303	1263.178	1423.428	1254.349	1407.703	1567.981	1198.738
Lymphatic nodes	153.525	178.358	202.461	174.831	198.930	223.439	197.573	220.962	245.457	189.649
Muscle	23916.788	27892.358	31746.357	27356.942	31222.064	35147.466	31037.554	34794.952	38724.357	29776.580
Oesophagus wall	41.731	48.753	55.556	47.768	54.590	61.516	54.209	60.836	67.763	51.805

(*Continued*)

Table 5. (*Continued*)

Organ/tissue	M_H10W10	M_H10W50	M_H10W90	M_H50W10	M_H50W50	M_H50W90	M_H90W10	M_H90W50	M_H90W90	MRCP (male)
Oesophagus contents	18.422	21.522	24.526	21.087	24.099	27.157	23.931	26.857	29.915	22.870
Gonads	28.776	33.618	38.309	33.249	37.998	42.818	38.129	42.790	47.662	37.234
Pancreas	139.864	163.400	186.200	160.098	182.965	206.176	181.686	203.899	227.114	173.634
Pituitary gland	0.572	0.601	0.632	0.604	0.631	0.664	0.637	0.664	0.696	0.622
Prostate	14.192	16.580	18.893	16.245	18.565	20.920	18.435	20.689	23.045	17.618
RST	11321.548	19019.906	31727.259	14735.951	21873.770	34675.484	17125.727	25026.275	37735.413	18212.525
Salivary glands	75.623	84.236	92.763	82.101	90.238	98.692	88.900	96.620	104.889	88.090
Skin	2959.467	3337.291	3785.683	3264.527	3624.888	4065.409	3579.808	3924.185	4350.814	3469.569
Spinal cord	30.916	35.826	40.595	35.017	39.763	44.593	39.382	43.972	48.783	37.952
Spleen	183.982	214.941	244.933	210.597	240.678	271.211	238.996	268.215	298.753	228.400
Thymus	20.870	24.382	27.785	23.890	27.302	30.765	27.111	30.426	33.890	25.909
Thyroid	18.809	21.975	25.041	21.530	24.606	27.727	24.434	27.421	30.543	23.351
Tonsils	2.751	2.986	3.225	2.949	3.172	3.410	3.156	3.369	3.603	3.109
Tongue	46.508	52.125	57.653	50.599	55.893	61.360	54.890	59.898	65.233	54.552
Tongue food	18.244	20.113	21.975	19.697	21.462	23.308	21.220	22.893	24.700	20.993
Teeth, retention	0.037	0.041	0.045	0.040	0.044	0.048	0.044	0.047	0.051	0.043
Ureter	13.357	15.605	17.782	15.289	17.473	19.690	17.351	19.472	21.689	16.582
Bladder wall	41.161	48.088	54.798	47.116	53.846	60.677	53.469	60.006	66.839	51.099
Bladder contents	161.105	188.214	214.478	184.411	210.751	237.488	209.278	234.864	261.605	200.000
Air inside body	0.123	0.134	0.146	0.133	0.144	0.156	0.144	0.155	0.166	0.140
Water	0.142	0.159	0.175	0.156	0.172	0.188	0.171	0.186	0.202	0.166
Body weight (g)	55897.502	70594.970	90191.182	64696.574	79294.236	99090.121	74195.791	88693.381	108389.121	72985.740
Target body weight (g)	55900.000	70600.000	90200.000	64700.000	79300.000	99100.000	74200.000	88700.000	108400.000	73000.000
Difference (%)	<0.05	<0.05	<0.05	<0.05	<0.05	<0.05	<0.05	<0.05	<0.05	<0.05
Standing height (cm)	167.2	167.2	167.2	176.5	176.5	176.5	185.8	185.8	185.8	176.0
Target standing height (cm)	167.2	167.2	167.2	176.5	176.5	176.5	185.8	185.8	185.8	176.0
Difference (%)	0.00	0.00	0.00	0.00	0.00	0.00	0.00	0.00	0.00	0.00

Table 6. Organ/tissue masses of constructed phantoms and the MRCP for adult female. Note that the organ/tissue masses are inclusive of blood content. (Unit: grams.)

Organ/tissue	F_H10W10	F_H10W50	F_H10W90	F_H50W10	F_H50W50	F_H50W90	F_H90W10	F_H90W50	F_H90W90	MRCP (female)
Adrenals	12.246	14.625	17.044	13.761	16.169	18.739	15.316	17.718	20.459	15.466
ET	16.332	18.136	20.065	17.423	19.192	21.169	18.526	20.244	22.286	19.078
Oral mucosa	0.085	0.096	0.108	0.091	0.102	0.114	0.097	0.108	0.120	0.101
Trachea	6.494	7.753	9.035	7.287	8.560	9.920	8.100	9.369	10.818	8.201
BB_1	1.062	1.268	1.478	1.193	1.402	1.624	1.328	1.536	1.774	1.340
Arteries	193.419	230.947	269.078	217.513	255.476	296.005	242.258	280.244	323.423	246.000
Veins	580.088	692.892	807.413	652.581	766.624	888.367	726.938	840.819	970.794	737.998
Skeletal system	5908.205	6923.715	7964.369	6565.304	7591.569	8694.399	7238.446	8260.771	9434.210	7285.617
Brain	1274.300	1305.545	1351.932	1325.615	1357.412	1404.929	1378.142	1409.975	1458.881	1349.568
Breasts, glandular	162.317	193.842	225.915	182.399	214.314	248.382	203.009	234.847	271.180	204.982
Breasts, adipose	193.525	311.138	566.309	224.210	343.767	593.420	255.026	373.511	618.360	307.326
Eye	13.863	14.722	15.742	14.620	15.470	16.515	15.391	16.223	17.301	15.366
Gallbladder wall	6.494	7.755	9.039	7.298	8.574	9.937	8.122	9.396	10.850	8.201
Gallbladder contents	38.009	45.391	52.901	42.712	50.185	58.162	47.538	54.993	63.501	48.000
Stomach wall	136.891	163.477	190.526	153.827	180.742	209.473	171.208	198.059	228.700	172.873
Stomach contents	182.127	217.499	253.486	204.660	240.470	278.695	227.785	263.509	304.276	230.000
Small intestine wall	598.461	714.691	832.942	672.502	790.171	915.763	748.482	865.870	999.834	757.768
Small intestine contents	221.720	264.782	308.592	249.151	292.746	339.281	277.303	320.793	370.423	280.000
Colon wall	356.536	425.745	496.228	400.645	470.684	545.533	445.891	515.815	595.616	450.252
Colon contents	253.397	302.611	352.680	284.747	334.570	387.754	316.921	366.624	423.344	320.003
Heart wall	230.344	275.065	320.569	258.841	304.131	352.477	288.088	333.270	384.892	290.890
Blood in heart	292.988	349.890	407.782	329.236	386.843	448.336	366.436	423.905	489.487	370.000
Kidneys	282.618	337.507	393.350	317.583	373.151	432.468	353.467	408.902	472.163	356.905
Liver	1433.264	1711.625	1994.826	1610.585	1892.392	2193.210	1792.567	2073.699	2394.519	1810.000
Lungs	752.086	898.153	1046.758	845.133	993.007	1150.858	940.625	1088.146	1256.492	949.774
Lymphatic nodes	120.212	142.415	165.082	134.346	156.783	180.808	148.857	171.209	196.786	150.958
Muscle	14087.812	16790.081	19541.581	15825.615	18563.093	21487.379	17616.144	20349.629	23470.999	17926.439
Oesophagus wall	34.227	40.858	47.605	38.396	45.099	52.253	42.672	49.350	56.958	43.219
Oesophagus contents	16.819	20.082	23.401	18.879	22.178	25.701	20.991	24.280	28.034	21.240

(*Continued*)

Table 6. (*Continued*)

Organ/tissue	F_H10W10	F_H10W50	F_H10W90	F_H50W10	F_H50W50	F_H50W90	F_H90W10	F_H90W50	F_H90W90	MRCP (female)
Gonads	10.006	11.950	13.927	11.244	13.212	15.312	12.515	14.478	16.717	12.636
Pancreas	114.464	136.695	159.312	128.626	151.132	175.156	143.159	165.611	191.233	144.552
Pituitary gland	0.558	0.590	0.628	0.588	0.619	0.659	0.618	0.649	0.689	0.615
Uterus	64.927	77.537	90.366	72.960	85.726	99.353	81.203	93.939	108.472	81.998
RST	14068.677	22618.673	41168.912	16299.431	24990.775	43139.786	18539.573	27153.040	44952.837	22325.388
Salivary glands	61.084	68.134	75.681	65.226	72.185	79.893	69.454	76.187	84.149	71.760
Skin	2025.482	2333.570	2794.238	2204.579	2507.756	2958.814	2382.952	2676.241	3120.932	2422.029
Spinal cord	15.303	18.060	20.877	16.980	19.749	22.717	18.695	21.439	24.581	19.098
Spleen	148.394	177.215	206.536	166.753	195.931	227.076	185.595	214.702	247.919	187.400
Thymus	16.235	19.388	22.596	18.244	21.436	24.844	20.305	23.490	27.124	20.503
Thyroid	15.406	18.398	21.442	17.312	20.341	23.574	19.268	22.290	25.738	19.455
Tonsils	2.628	2.923	3.237	2.805	3.094	3.415	2.984	3.264	3.596	3.075
Tongue	33.519	38.246	43.155	36.012	40.640	45.676	38.529	43.013	48.218	40.415
Tongue food	17.827	19.936	22.166	19.052	21.119	23.405	20.292	22.295	24.656	20.995
Teeth, retention	0.030	0.034	0.038	0.033	0.036	0.040	0.035	0.038	0.043	0.036
Ureter	12.176	14.541	16.947	13.683	16.077	18.633	15.229	17.617	20.343	15.378
Bladder wall	32.311	38.587	44.971	36.309	42.662	49.444	40.412	46.749	53.982	40.805
Bladder contents	158.372	189.130	220.423	177.965	209.104	242.344	198.074	229.138	264.588	200.000
Air inside body	0.030	0.034	0.038	0.033	0.037	0.041	0.036	0.039	0.044	0.036
Water	0.097	0.109	0.121	0.104	0.115	0.128	0.111	0.122	0.136	0.114
Body weight (g)	44203.470	58206.056	82611.448	49904.092	64106.623	88411.979	55704.715	69807.157	94112.478	60001.848
Target body weight (g)	44200.000	58200.000	82600.000	49900.000	64100.000	88400.000	55700.000	69800.000	94100.000	60000.000
Difference (%)	<0.05	<0.05	<0.05	<0.05	<0.05	<0.05	<0.05	<0.05	<0.05	<0.05
Standing height (cm)	154.9	154.9	154.9	163.3	163.3	163.3	171.7	171.7	171.7	163.0
Target standing height (cm)	154.9	154.9	154.9	163.3	163.3	163.3	171.7	171.7	171.7	163.0
Difference (%)	0.00	0.00	0.00	0.00	0.00	0.00	0.00	0.00	0.00	0.00

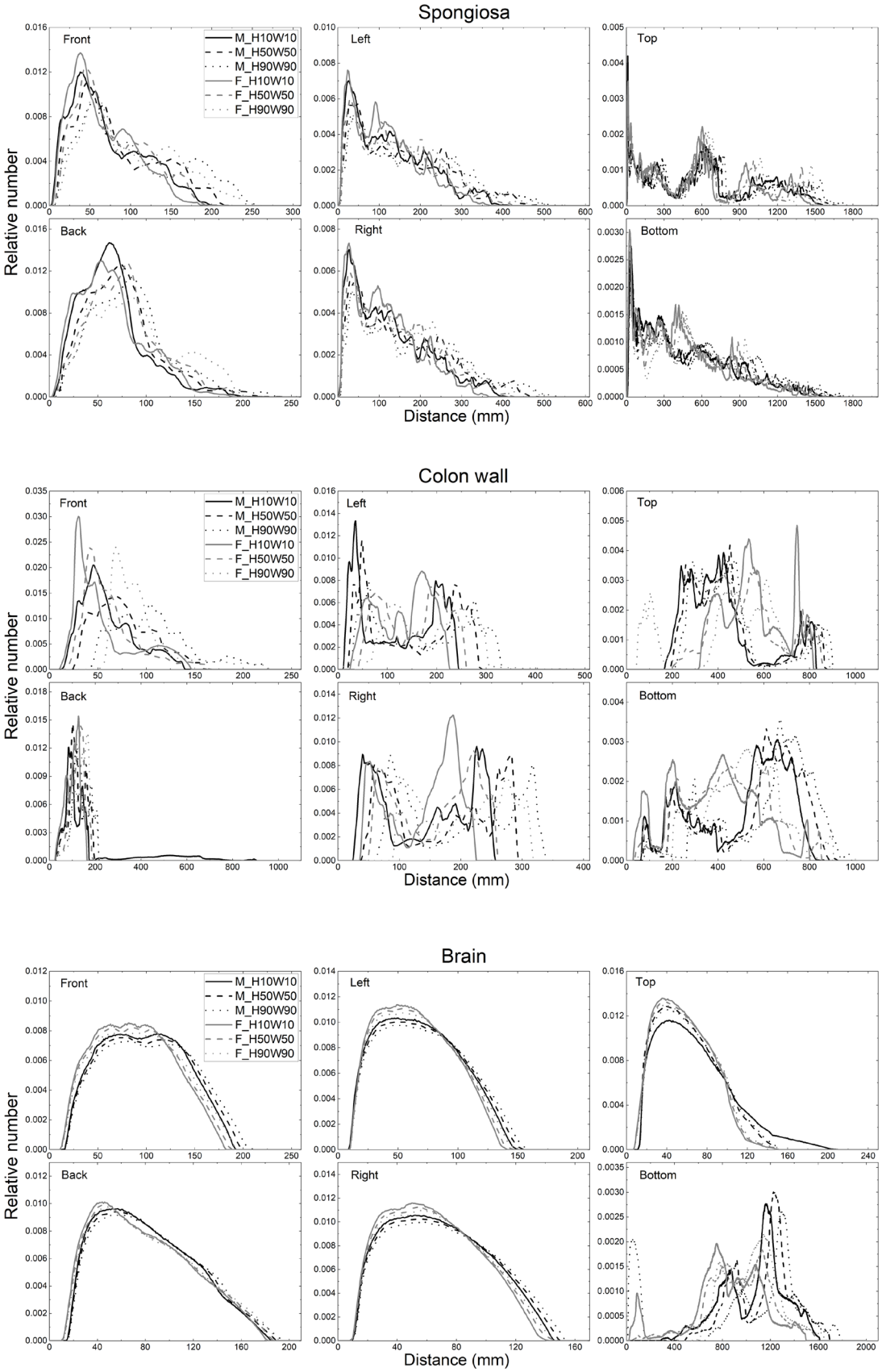

Figure 4. Organ-depth distributions (ODDs)—the distributions of depths of 10^7 randomly sampled points in selected organs (spongiosa, colon wall, and brains) below the body surfaces at: front, back, left, right, top, and bottom for M_H10W10, M_H50W50, M_H90W90, F_H10W10, F_H50W50, and F_H90W90 phantoms.

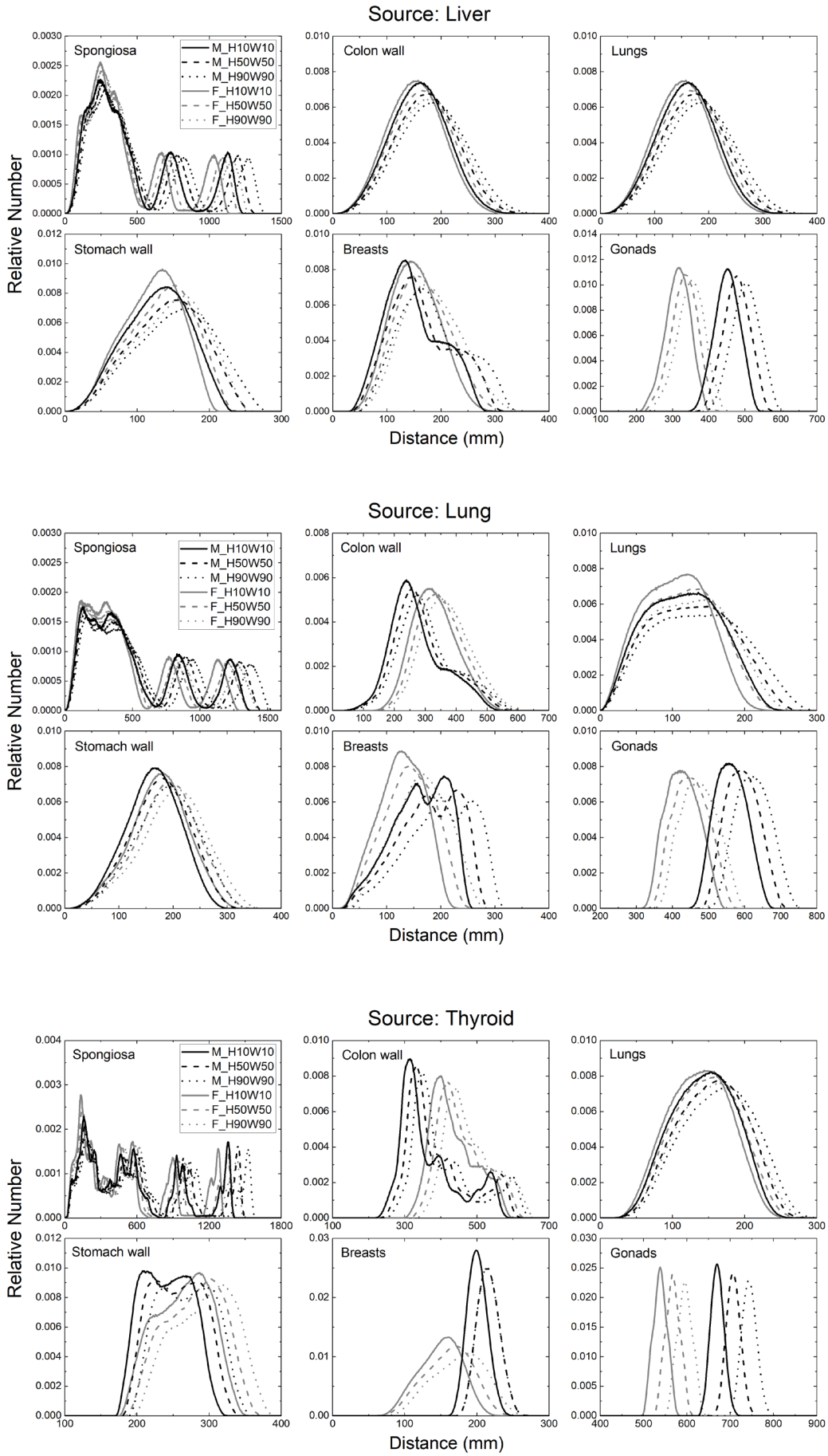

Figure 5. Chord-length distributions (CLDs)—the distributions of distances between 10^7 randomly sampled point pairs in selected source regions (liver, lungs, and thyroid) and target regions (spongiosa, colon wall, lungs, stomach wall, breasts, and gonads) for M_H10W10, M_H50W50, M_H90W90, F_H10W10, F_H50W50, and F_H90W90 phantoms.

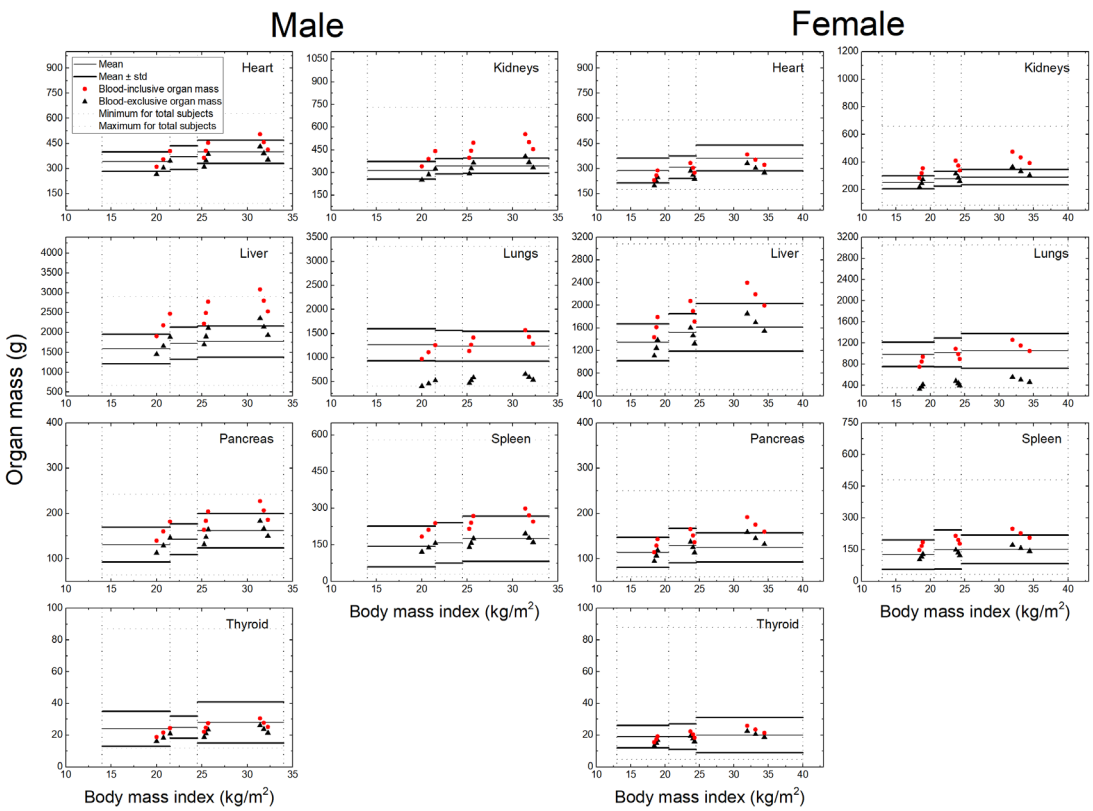

Figure 6. Comparison of organ masses of percentile-specific phantoms with autopsy data according to body mass index (BMI).

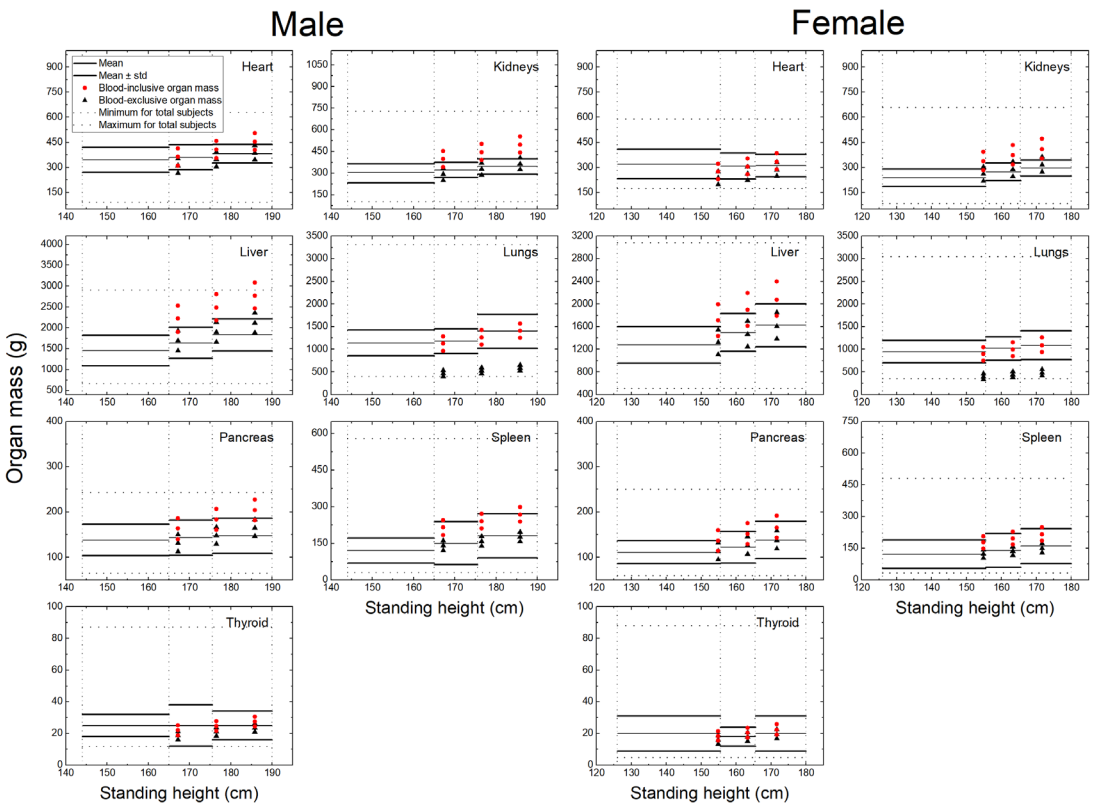

Figure 7. Comparison of organ masses of percentile-specific phantoms with autopsy data according to standing height.

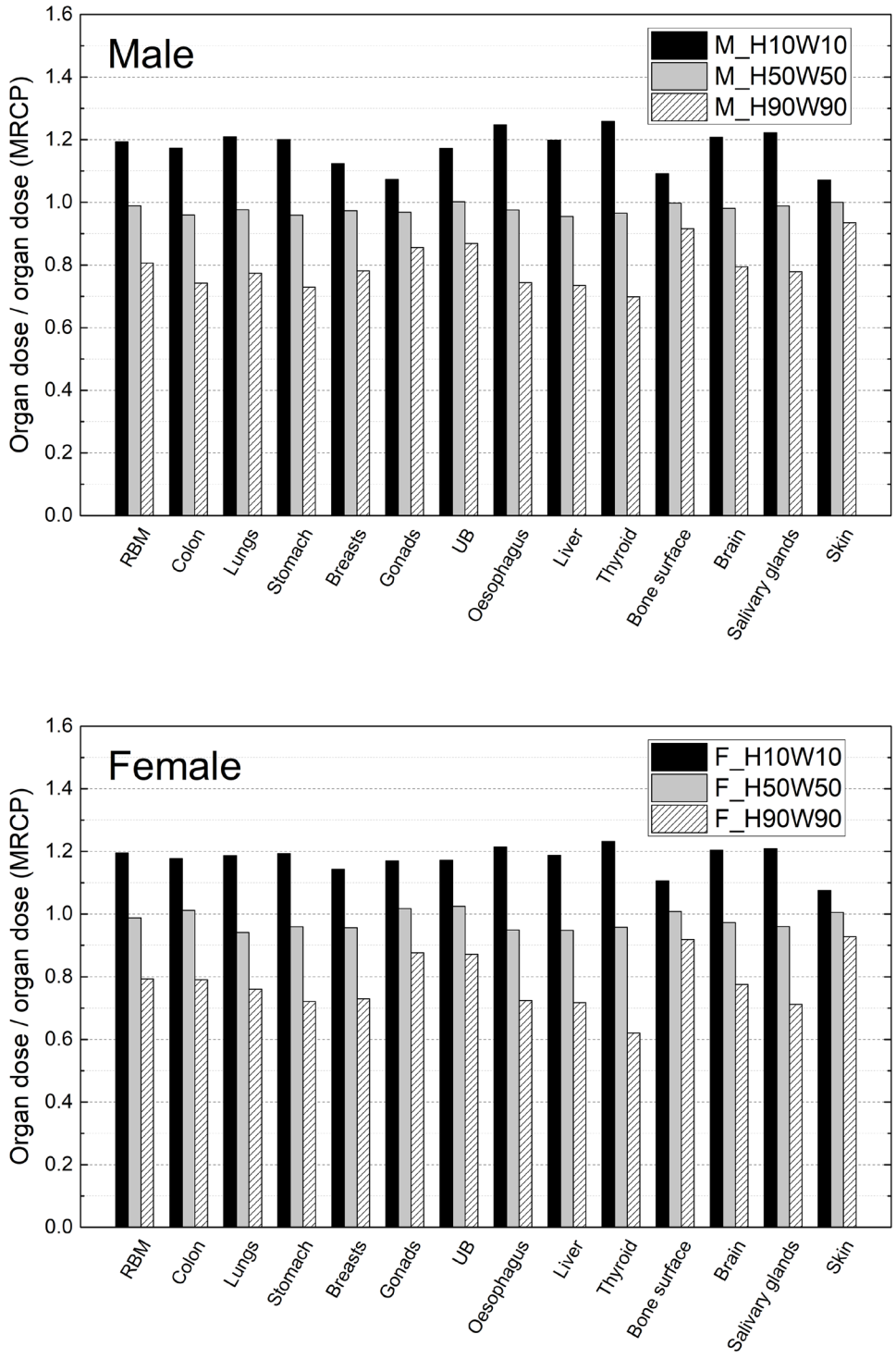

Figure 8. Comparison of organ doses (=organ or tissue-averaged absorbed doses) of H10W10, H50W50, and H90W90 percentile-specific phantoms with those of the MRCPs for male (upper) and female (lower) for gamma irradiation by cesium-137 contamination on floor. Bar graph shows ratios of organ dose of percentile-specific phantom to organ dose of the MRCP for selected organs and tissues.

dimensions increase by only about 6–7%, while the other secondary anthropometric parameters increase by ~30%. For the bottom direction, the ODDs are significantly different even for the brain for different percentile phantoms, which reflects the differences in standing heights for different percentile phantoms.

Figure 5 shows the chord-length distributions (CLDs) for selected source regions (liver, lungs, and thyroid) and target regions (spongiosa, colon wall, lungs, stomach wall, breasts, and gonads) for M_H10W10, M_H50W50, M_H90W90, F_H10W10, F_H50W50, and F_H90W90 percentile-specific phantoms. For the CLD calculation, 10^7 point pairs were randomly sampled in the considered target and source regions, and distances of the point pairs were calculated. The CLDs represent a distance between the target and source regions, influencing

dose calculation for internal exposure. Again, the CLDs well reflect the scaling of the phantoms in the axial and transversal directions, the broadening of the CLDs mainly depending on the sizes of the phantoms.

3.4. Organ mass comparison with autopsy data

In the present study, the organ masses of the constructed phantoms were compared with the data of a French-based autopsy (de la Grandmaison *et al* 2001), in which 684 subjects were assembled into three groups, according to the body mass index (BMI) and the standing height, and then mean organ masses and their standard deviations were obtained for each group through forensic autopsy. Note that while organs of the phantoms were constructed considering the included blood contents, the organ masses of the autopsy data are generally between the masses *in vivo* (blood-inclusive) and parenchymal masses (blood-exclusive) because of the blood loss during the autopsy procedures. Lung mass of the autopsy data, however, is rather closer to the blood-inclusive mass, due to the autopsy techniques used by de la Grandmaison *et al* (2001) which presumed the lung mass inclusive of blood (ICRP 2002). For the consideration of the blood contents included in the organs, in the present study, blood-exclusive organ masses were additionally derived for analysis purpose, by subtracting blood content mass included in each organ calculated by the proportions of regional blood content of each organ of the MRCPs.

Figures 6 and 7 show the organ masses (blood-inclusive) of the constructed phantoms and the organ masses of the autopsy data, together with derived blood-exclusive organ masses, for the heart, kidneys, liver, lungs, pancreas, spleen and thyroid, according to the BMI and the standing height. For the heart, lungs, pancreas, spleen, and thyroid, the organ masses of the constructed phantoms tend to be larger than the autopsy values, but generally stay within one or two standard deviations from the mean of the autopsy data. On the other hand, the liver and kidney masses of the constructed phantoms show relatively large deviations from the autopsy data. These deviations can be explained by the fact that the organ masses of the MRCPs are the masses fully including regional blood content, unlike organ masses obtained by the autopsy. Note that, according to the data in ICRP Publication 89 (2002), the inclusion of regional blood content in the liver increases the liver mass by 31% and 29% for male and female, respectively, and the inclusion of the blood content in the kidneys increases the kidney mass by 36% and 30% for male and female. In addition, although the blood-inclusive organ masses are relatively larger than the autopsy data, the blood-exclusive organ masses of liver and kidney stay within one or two standard deviations from the mean of the autopsy data. Therefore, it can be generally concluded that the organ masses of the constructed phantoms are within reasonable ranges.

3.5. Comparison of organ doses

The M_H10W10, M_H50W50, M_H90W90, F_H10W10, F_H50W50, and F_H90W90 percentile-specific phantoms were implemented in the Geant4 Monte Carlo code to calculate organ/tissue doses for exposures from a cesium-137 contaminated floor and the calculated organ/tissue doses were compared with those of the MRCPs. Figure 8 shows the ratios of the organ absorbed dose of a percentile-specific phantom and that of the MRCP for selected organs.

The results showed that organ absorbed doses of the 50th percentile phantoms (i.e. M_H50M50 and F_H50M50) are indeed very close to those of the MRCPs, generally differences being less than 10%. In particular, the organs/tissues with relatively large tissue weighting factor ($w_T \geqslant 0.08$) (i.e. RBM, colon, lungs, stomach, breasts, and gonads) show minimal differences, i.e. less than 5%. Therefore, although the body weight of the MRCPs is less than those of the 50th percentile phantoms by 6.3 kg and 4.1 kg for the male and female phantom, respectively, it can be concluded that, for at least this case, the MRCPs properly represent the Caucasian population for radiation protection purpose.

On the other hand, there were noticeable differences of the organ absorbed doses for the 10th and 90th percentile phantoms when compared to the MRCPs. The 10th percentile phantom receives higher doses for all organs/tissues than the MRCPs, with maximum differences of 26% and 23% (in thyroid dose) for the male and female phantom, respectively. On the contrary, the 90th percentile phantom receives lower doses than the MRCPs, with maximum differences of 30% and 38% (in thyroid dose) for the male and female phantom, respectively. These results confirm the general intuition that a small person receives higher doses than a large person when exposed to a static radiation field; and organs closer to the source receive higher absorbed doses.

4. Conclusion

In the present study, the adult MRCPs were deformed to produce a set of percentile-specific adult phantoms which represent 10th, 50th and 90th percentile standing heights and body weights in adult male female Caucasian populations. For this phantom construction, the anthropometric parameters were first derived for the percentile-specific phantoms, and the MRCPs were matched to the parameters to produce percentile-specific phantoms. Then, the effect and validity of scaling and adjustments were investigated by calculating organ depth and cord length distributions and by comparing the organ masses with available autopsy data. The constructed phantoms

were also used to calculate organ doses for a cesium-137 contaminated floor, and the calculated values were compared with those of the MRCPs. The results of dose calculations showed that the organ doses of the 50th percentile (i.e. M_H50M50 and F_H50M50) phantoms are close to those of the MRCPs. However, there were noticeable differences of the organ doses for the 10th and 90th percentile phantoms when compared to the MRCPs, confirming the general intuition that a small person receives higher doses than a large person when exposed to a static radiation field; and organs closer to the source receive higher absorbed doses. In the near future, the methodology developed in the present study will be automated to produce a phantom library with various body sizes, for which manual deformation is not acceptable considering the number of phantoms to be produced.

Acknowledgments

The authors thank Hyojoo Kim, Jong Chan Jung, Sang Hyun Jun and Jeong Yeol Baek, in the Department of Nuclear Engineering at Hanyang University in Seoul, Korea, for their time and efforts to construct percentile-specific phantoms. This work was supported by Nuclear Safety Research Development (NSR&D) Program through Korea Foundation of Nuclear Safety (KoFONS), funded by the Nuclear Safety and Security Commission (NSSC), and additionally, by the National Research Foundation of Korea (NRF) funded by the Ministry of Science, ICT and Future Planning through the National Research Foundation of Korea (Project No.: 1705006, 2016R1D1A1A09916337). Two of the authors (Chansoo Choi and Haegin Han) were supported by the Global PhD Fellowship program (Project No.: NRF-2017H1A2A1046391, NRF-2018H1A2A1059767), and one of the authors (Yeon Soo Yeom) was supported by a grant of the Korean Health Technology R&D Project through the Korean Health Industry Development Institute (KHIDI), funded by the Ministry of Health & Welfare, Republic of Korea (Project No: H18C2257).

ORCID iDs

Hanjin Lee https://orcid.org/0000-0002-6710-8767
Yeon Soo Yeom https://orcid.org/0000-0001-5373-6693
Chansoo Choi https://orcid.org/0000-0002-8203-9835

References

Akhavanallaf A, Xie T and Zaidi H 2018 Development of a library of adult computational phantoms based on anthropometric indexes *IEEE. Trans. Radiat. Plasma Med. Sci.* **3** 65–75

Allison J, Amako K, Apostolakis J, Arce P, Asai M, Aso T, Bagli E, Bagulya A, Banerjee S and Barrand G 2016 Recent developments in Geant4 *Nucl. Instrum. Methods Phys. Res.* A **835** 186–225

Bochud F O, Laedermann J P, Baechler S, Bailat C J, Boschung M, Aroua A and Mayer S 2014 Monte Carlo simulation of a whole-body counter using IGOR phantoms *Radiat. Prot. Dosim.* **162** 280–8

Boer P 1984 Estimated lean body mass as an index for normalization of body fluid volumes in humans *Am. J. Physiol. Renal Physiol.* **247** 632–6

Bosy-Westphal A, Reinecke U, Schlo¨rke T, Illner K, Kutzner D, Heller M and Müller M J 2004 Effect of organ and tissue masses on resting energy expenditure in underweight, normal weight and obese adults *Int. J. Obes.* **28** 72–9

Cassola V F, Milian F M, Kramer R, de Oliveira Lira C A B and Khoury H J 2011 Standing adult human phantoms based on 10th, 50th and 90th mass and height percentiles of male and female Caucasian populations *Phys. Med. Biol.* **56** 3749–72

Chen Y, Qiu R, Li C, Wu Z and Li J 2016 Construction of Chinese adult male phantom library and its application in the virtual calibration of *in vivo* measurement *Phys. Med. Biol.* **61** 2124–44

Clairand I, Huet C, Trompier F and Bottollier-Depois J F 2008 Physical dosimetric reconstruction of a radiological accident due to gammagraphy equipment that occurred in Dakar and Abidjan in summer 2006 *Radiat. Meas.* **43** 698–703

Courageot E, Huet C, Clairand I, Bottollier-Depois J F and Gourmelon P 2010 Numerical dosimetric reconstruction of a radiological accident in South America in April 2009 *Radiat. Prot. Dosim.* **144** 540–2

de la Grandmaison G L, Clairand I and Durigon M 2001 Organ weight in 684 adult autopsies: new tables for a Caucasoid population *Forensic Sci. Int.* **119** 149–54

Deurenberg P, Weststrate J A and Seidell J C 1991 Body mass index as a measure of body fatness: age- and sex-specific prediction formulas *Br. J. Nutr.* **65** 105–14

Ding A, Mille M M, Liu T, Caracappa P F and Xu X G 2012 Extension of RPI-adult male and female computational phantoms to obese patients and a Monte Carlo study on the effects on CT imaging dose *Phys. Med. Biol.* **57** 2441–59

Eakins J S and Kouroukla E 2015 Luminescence-based retrospective dosimetry using Al_2O_3 from mobile phones: a simulation approach to determine the effects of position *J. Radiol. Prot.* **35** 343–81

Geyer A M, O'Reilly S, Lee C, Long D J and Bolch W E 2014 The UF/NCI family of hybrid computational phantoms representing the current US population of male and female children and adolescents—applications to CT dosimetry *Phys. Med. Biol.* **59** 5225–42

Gordon C C *et al* 2014 2012 anthropometric survey of U.S. army personnel: methods and summary statistics (NATICK/TR-15/007) U.S. Army Natick Soldier Research, Development and Engineering Center, Natick, MA (https://apps.dtic.mil/docs/citations/ADA611869)

Hume R 1966 Prediction of lean body mass from height and weight *J. Clin. Pathol.* **19** 389–91

ICRP 1975 Report of the Task Group on Reference Man. ICRP Publication 23 *Ann. ICRP* **4** (Oxford: Pergamon)

ICRP 2002 Basic Anatomical and Physiological Data for Use in Radiological Protection: Reference Values. ICRP Publication 89 *Ann. ICRP* **32** (Oxford: Pergamon)

ICRP 2009 Adult Reference Computational Phantoms. ICRP Publication 110 *Ann. ICRP* **39** (Amsterdam: Elsevier)

ICRP 2010 Conversion Coefficients for Radiological Protection Quantities for External Radiation Exposures. ICRP Publication 116 *Ann. ICRP* 40 (Amsterdam: Elsevier)
James W P T and Waterlow J C 1976 Research on Obesity: A Report of the DHSS/MRC Group (London: HM Stationery Office)
Johnson P B, Whalen S R, Wayson M, Juneja B, Lee C and Bolch W E 2009 Hybrid patient-dependent phantoms covering statistical distributions of body morphometry in the US adult and pediatric population *Proc. IEEE* **97** 2060–75
Kim C H *et al* 2018 New mesh-type phantoms and their dosimetric applications, including emergencies *Ann. ICRP* **47** 45–62
Lu W, Wu Z, Qiu R, Li C, Yang B, Gao S, Ren L and Li J 2017 Physical dosimetric reconstruction of a radiological accident at Nanjing (China) for clinical treatment using Thudose *Health Phys.* **113** 327–34
McArdle W D, Katch F I and Katch V L 2006 *Essentials of Exercise Physiology* (Philadelphia: Lippincott Williams & Wilkins)
Na Y H, Zhang B, Zhang J, Caracappa P F and Xu X G 2010 Deformable adult human phantoms for radiation protection dosimetry: anthropometric data representing size distributions of adult worker populations and software algorithms *Phys. Med. Biol.* **55** 3789–811
Pierrat N, de Carlan L, Cavadore D and Franck D 2005 Application of Monte Carlo calculation for the virtual calibration of a low-energy *in vivo* counting system *IEEE Trans. Nucl. Sci.* **52** 1353–8
Pieterman R, Willemsen A, Appel M, Pruim J and Koëter G 2002 Visualisation and assessment of the protein synthesis rate of lung cancer using carbon-11 tyrosine and positron emission tomography *Eur. J. Nucl. Med. Mol. Imaging* **29** 243–47
Qiu R, Li J, Zhang Z, Wu Z, Zeng Z and Fan J 2008 Photon SAF calculation based on the Chinese mathematical phantom and comparison with the ORNL phantoms *Health Phys.* **95** 716–24
Si H 2015 TetGen, a Delaunay-based quality tetrahedral mesh generator *ACM Trans. Math. Softw.* **41** 1–36
UN-DESA 2017 United Nations, Department of Economic and Social Affairs, Population division 2017 World Population Prospects: the 2017 revision, DVD edition (https://population.un.org/wpp/Download/Standard/Population)
Yeom Y S, Jeong J H, Han M C and Kim C H 2014 Tetrahedral-mesh-based computational human phantom for fast Monte Carlo dose calculations *Phys. Med. Biol.* **59** 3173–85